HHS Public Access

Author manuscript

*Exp Eye Res*. Author manuscript; available in PMC 2017 May 01.

Published in final edited form as:

*Exp Eye Res*. 2016 May ; 146: 354–360. doi:10.1016/j.exer.2016.01.008.

# Variations in Active Outflow Along the Trabecular Outflow Pathway

**Elliott D.K. Cha**[1], **Jia Xu**[1], **Lihua Gong**[1,2], and **Haiyan Gong**[1]

[1]Boston University School of Medicine, Department of Ophthalmology Boston, MA, USA

[2]Ophthalmology, Qingpu Branch of Zhongshan Hospital Affiliated to Fudan Universtiy, Shanghai, China

## Abstract

Previous tracer studies have shown segmental outflow in the trabecular meshwork (TM) and along the inner wall (IW) of Schlemm's canal (SC). Whether segmental outflow is conserved distal to SC has not yet been investigated. This study aims to investigate whether the segmented pattern of outflow is conserved in distal outflow pathways by using a newly developed global imaging method and to evaluate variations of active outflow in three distinct regions along trabecular outflow pathway.

Six normal whole globe human eyes were first perfused at 15mmHg to establish a stable baseline outflow facility. The anterior chamber was then exchanged (5 mL) and perfused with fluorescent microspheres (0.002% v/v, 200μL) to label areas of active outflow. All eyes were perfusion fixed and dissected into anterior segments. The TM and scleral surface were *en face* imaged globally. Effective filtration area (EFA) and fluorescent tracer distribution and intensity were analyzed in global images for both the TM and episcleral veins (EPVs). Anterior segments were further dissected into a minimum of 16 radial wedges, from which frontal sections were cut, stained, and imaged, using confocal microscopy. EFA from all three locations along the trabecular outflow pathway were measured and compared. Additionally, TM thickness, SC height, and total number of collector channels (CC) were analyzed and compared between active and inactive areas of outflow. Statistical analysis was performed using Student's t-tests and Wilcoxon signed-rank test with a required significance of $p \leq 0.05$.

All three locations showed a segmental outflow pattern. The TM had a significantly higher mean EFA (86.3±3.5%) compared to both the IW (34.7±2.9%; $p \leq 0.01$) and EPVs (41.1±3.8%; $p \leq 0.01$). No significant difference in mean EFA was found between IW and EPVs. Preferential active outflow was observed in the nasal and inferior quadrants. TM thickness was significantly larger in areas of active outflow (103.3±4.0 μm; $p \leq 0.01$) compared to areas of inactive outflow (78.5±6.5 μm), but there was no significant difference in SC height between active and inactive outflow areas. Among all eyes, a total of 80 CCs were counted with 63 associated with active outflow and

Corresponding Author: Dr. Haiyan Gong, Department of Ophthalmology, Boston University School of Medicine, 72 E. Concord St. Room L-905, Boston, MA 02118, (617) 638-4434, ; Email: hgong@bu.edu

17 associated with inactive outflow. A higher number of CCs associated with areas of active outflow were found in the nasal (26 of 63) and inferior (20 of 63) quadrants compared to the temporal (9 of 63) and superior (8 of 63) quadrants.

A segmental nature of outflow is conserved along the trabecular outflow pathway with variations in three distinct locations (TM, IW, and EPVs). IW and EPVs showed a similar mean EFA. Preferential active outflow was observed in the nasal and inferior quadrants of the eye, which are associated with more expanded TM and higher number of CCs. Normal outflow patterns and its variations along the outflow pathway reported in this study will provide the basis for future studies of the outflow changes in eyes with glaucoma.

**Keywords**

segmental outflow; trabecular meshwork; Schlemm's canal; collector channels; episcleral veins; imaging; confocal microscopy

## 1. Introduction

Normal intraocular pressure (IOP) is maintained through a dynamic balance between the amount of aqueous humor production and drainage. Dysfunction or impairment of the aqueous outflow drainage pathway due to increased outflow resistance results in elevated IOP, which is a primary risk factor for primary open angle glaucoma (POAG). The majority of aqueous humor (50 – 80%) is removed through the trabecular outflow pathway (Bill 1965, Bill and Hellsing 1965, Toris et al. 1999) and several previous studies have localized the primary site of outflow resistance to a thin region of tissue within the trabecular meshwork (TM), that includes the inner wall (IW) endothelium of Schlemm's canal (SC) and its basement membrane, as well as the underlying juxtacanalicular connective tissue (JCT) (Grant 1958, Grant 1963, Maepea and Bill 1989, Maepea and Bill 1992). However, following complete trabeculotomy at normal IOP (7mmHg) in enucleated human eyes, only 49% of outflow resistance was eliminated and at a higher IOP (25mmHg) 71% of outflow resistance was eliminated (Rosenquist et al. 1989). Additionally, Schuman et al. (1999) reported that following a 1-clock hour ablation of the tissue distal to the outer wall of SC, using an excimer laser at a perfusion pressure of 10mmHg, 35% of outflow resistance was eliminated. Collectively, these studies suggest that one-third to one-half of the outflow resistance lies distal to the IW of SC at various pressures. However, the mechanism by which outflow resistance is generated and regulated in each location remains unclear and is even further complicated by segmental flow.

Earlier tracer studies using electron microscopy in monkey (MacRae and Sears 1970, Epstein and Rohen 1991, Sabanay et al. 2000) and human eyes (MacRae and Sears 1970, de Kater et al. 1989, Ethier and Chan 2001, Hann et al. 2005) found variable distribution of outflow tracers within the TM and along the abluminal and luminal side of the IW of SC. While these observations were the first to describe the non-uniform or segmental outflow, as labeled by various tracers, it also suggested that outflow resistance might vary in different locations along the limbus. A limitation of these studies was that only a small fraction of the TM along the circumference of the limbus was examined by electron microscopy. More

recent studies took on a more macroscopic approach to visualizing outflow patterns in larger areas within the TM and along the IW by combining the use of fluorescent microspheres and confocal microscopy. It was found that even on a larger scale, outflow patterns remained segmental in both non-human (Lu et al. 2007, Battista et al. 2008, Lu et al. 2008, Zhu et al. 2010) and human eyes (Keller et al. 2011, Yang et al. 2013, Chang et al. 2014). In order to understand how segmental outflow is regulated, more recent studies have begun to explore the potential mechanisms that contribute to this pattern and its association with outflow resistance. In particular, differences in both morphology and extracellular matrix composition have been associated with high and low flow regions of outflow in both human (Keller et al. 2011, Yang et al. 2013, Vranka et al. 2015) and mouse eyes (Swaminathan et al. 2013). Additionally, an inverse relationship between the percent of the effective filtration area (EFA) and outflow resistance was also found in non-human (Lu et al. 2007, Battista et al. 2008, Lu et al. 2008, Scott et al. 2009, Zhu et al. 2010) and human eyes (Yang et al. 2013).

Despite numerous studies looking at the segmental outflow patterns within the TM and along the IW, whether this same pattern is conserved distal to SC on a whole eye scale has not yet been investigated. Therefore, the aims of this study are: 1) To evaluate whether the segmented nature of outflow is conserved in distal outflow pathways by using our newly developed global imaging method; 2) To compare variations of areas of active outflow along the entire trabecular outflow pathway in three distinct locations (TM, IW, episcleral veins); and 3) Investigate which structures may contribute to the segmental pattern of outflow.

## 2. Materials and Methods

A total of 3 pairs of human eyes (N=6) were used in this study with an age range of 74 – 78 years old (76±2; Mean±SD). Whole globe human eyes were received from the National Disease Research Interchange (Philadelphia, PA) within 24-hours post-mortem and inspected for any physical damage under a dissecting microscope. Criteria for acceptable globes included a clear history of no diabetes, no chemotherapy within 1 year, and no history of known ocular diseases or surgeries.

### 2.1 Ocular Perfusion

Whole globe ocular perfusion was carried out using a similar protocol previously established (Scott et al. 2009). Briefly, all eyes were first perfused with a perfusion fluid containing 5.5 mM D-glucose + Dulbecco's phosphate buffered saline (DPBS) for 30 minutes at constant pressure (15mmHg) to establish a stable baseline outflow facility. Following establishment of baseline outflow facility, the anterior chamber fluid was exchanged with 5mL of carboxylated polystyrene fluorescent microspheres (0.002% v/v, 500nm, Life Technologies, Grand Island, NY) and additionally perfused with a fixed volume (200μL) of the same solution to label areas of active outflow. Once perfusion of microspheres was completed, the anterior chamber fluid was exchanged with 5mL of modified Karnovsky's fixative and perfusion-fixed for 30 minutes. A small equatorial cut was then made and eyes were additionally immersion-fixed overnight and stored in DPBS at 4°C until further processed.

### 2.2 Global Imaging

To image active outflow patterns in the entire trabecular meshwork (TM) and episcleral veins (EPV) from anterior segments of each eye, fixed whole globes (N=6) were first oriented into four quadrants (nasal, inferior, temporal, superior) based on the location of extra ocular muscle tissue, optic nerve head and macula lutea. Eyes were then dissected along the equator into an anterior and posterior segment. Anterior segments were retained and further processed by removing the iris, ciliary body, cornea (10 mm trephine), vitreous, and excess conjunctiva. Processed anterior segments were then imaged *en face* on both their TM and scleral surfaces with a fixed exposure time of 5 seconds (Fig. 1A) through a 300mm lens on a 4000MP VersaDock imaging system (Bio-Rad Laboratories, Hercules, CA) using Quantity One (Bio-Rad Laboratories, Hercules, CA).

### 2.3 Analysis of Areas of Active Outflow from Global Images

Fluorescent tracer distribution and intensity in the TM and EPVs of each global image was analyzed for areas of active outflow. To avoid identifying the auto-fluorescent sclera as a false positive, each global image underwent background subtraction using a fixed value (60 pixels) in Fiji (NIH, Bethesda, MD). Images were then digitally separated into a minimum of 16 different “wedges” (Fig. 1B) and analyzed for areas of active outflow using two different approaches.

The first approach was to quantify the percent of the scleral and TM surfaces that showed fluorescing tracers. We termed this measurement the effective filtration area (EFA). To calculate whole eye EFA, global images of the TM and scleral surfaces were measured for the total scleral length (TSL) and total filtration (tracer-labeled) length (TFL) along the circumference of the eye. Only one measurement for TSL and TFL was taken from global images of the TM surface (Fig. 2A), while three different measurements (inner, middle, outer) for TSL and TFL were taken from global images of the scleral surface (Fig. 2B). The average of three measurements was used to account for a larger scleral area compared to one measurement for the TM. EFA was calculated as $EFA = 100 X (\Sigma TFL/\Sigma TSL)$.

The second approach was to evaluate both the distribution and intensity of fluorescent tracers in the TM and EPVs. Each digital wedge was graded for fluorescent distribution and intensity using a grading system described in Table 1. Grading of the TM surface was restricted to only one area (Fig. 3A) whereas grading of EPVs took into account the entire anterior segment scleral surface of each eye (Fig. 3B). Each assessment was masked and performed by at least two independent evaluators and repeated twice in two separate sessions at least one week apart. Both inter and intra-observer comparisons had less than 10% variations. Image analysis for both approaches was done using Fiji (NIH, Bethesda, MD).

### 2.4 Confocal Microscopy and Analysis

Following global imaging and analysis, each anterior segment was further dissected into a minimum of 16 radial wedges, from which frontal sections were cut along a plane tangential to the corneoscleral limbus and perpendicular to the ocular surface ([Parc et al. 2000](), [Lu et al. 2008]()). Each wedge was first cut in the middle of SC followed by an anterior and posterior

cut parallel to the middle of SC. A minimum of 11 radial wedges (min. 2 per quadrant) per eye were cut into frontal sections. Each frontal section was permeabilized for 10 minutes with 0.01% (v/v) Triton X-100 (Sigma Aldrich, St. Louis, MO) and nuclear stained with either DAPI (Sigma Aldrich, St. Louis, MO) or TO-PRO 3 Iodide (Life Technologies, Grand Island, NY) for 10 minutes and washed twice with DPBS. Sections were then imaged in z-stacks (z resolution = 1.75 μm) using a 20x objective.

All frontal images (n=72) were subcategorized into groups of active or inactive outflow based on the presence or absence of fluorescent tracers in the TM, IW, and EPV. Outflow area was considered active when fluorescent tracers were present either in all three locations or in both the TM and along the IW. Outflow was considered inactive if fluorescent tracers were not found in all three locations or only found in the inner TM or uveal TM, or EPVs alone. A summary of the outflow types can be found in Table 2.

Following categorization, images were analyzed for the one-dimensional equivalent of EFA. Using a method previously described (Yang et al. 2013), each frontal image was measured for both total IW length (TL) and fluorescent-decorated length (FL) of the IW of SC (Fig. 2C). EFA was then calculated as EFA = 100 x ($\Sigma$FL/$\Sigma$TL). TM thickness was measured between the IW endothelium of SC to the innermost uveoscleral beam; and SC height was measured from the inner wall to the outer wall. Each measurement was conducted per 200 μm length of the IW for all images showing a complete TM. Lastly, the total number of collector channels for all eyes were counted and analyzed for their relationship with areas of active and inactive outflow.

All images were captured using an Axiovert LSM 700 (Carl Zeiss, Germany) in ZEN 2010 (Carl Zeiss, Germany) and measurements were performed using ZEN 2010 (Carl Zeiss, Germany).

### 2.5 Statistical Analysis

A paired two-tailed Student's t-test was used to analyze any post-baseline outflow facility changes. Inter-comparisons of EFA measured for the TM, IW, and EPVs from each radial wedge were done using a paired two-tailed Student's t-test. An unpaired two-tailed Student's t-test was used to analyze TM thickness and SC height from active and inactive outflow groups. A Wilcoxon signed-rank test was performed between all four quadrants to determine significant differences in mean values of fluorescent tracer distribution and intensity. Significance was defined as $p \leq 0.05$ for all tests.

## 3. Results

### 3.1 Outflow Facility

Average baseline outflow facility (N=6) was 0.19±0.05 μL/min/mmHg (Mean±SD), with no significant changes in post-baseline outflow facility after perfusion of fluorescent tracers ($p \geq 0.05$).

### 3.2 Comparison of Areas of Active Outflow in the TM, IW, and EPVs

First, EFA, in three different locations (TM, IW, and EPV) along the trabecular outflow pathway, was analyzed and compared using both global and confocal images. Segmental patterns of outflow were observed in all three locations with a significantly higher EFA in the TM (86.3±3.5%) (Mean±SE) compared to both the IW (34.7±2.9%; $p \leq 0.01$) and distal EPVs (41.1±3.8%; $p \leq 0.01$) (Fig. 4A – D). No significant differences in EFA were found between the IW and EPVs ($p=0.12$) (Fig. 4D).

Fluorescent tracer distribution and intensity in the TM and EPVs was further evaluated in all quadrants of global images using a grading system (Table 1). In the TM, no significant differences in fluorescent distribution and intensity were found between the nasal, inferior, and superior quadrants; however, the temporal quadrant showed a significantly lower mean value compared to the nasal quadrant only ($p \leq 0.05$) (Fig. 5A). Additionally, when compared to the temporal quadrant, the superior and inferior quadrants both showed a higher mean value for fluorescent distribution and intensity in the TM but did not reach statistical significance ($p \geq 0.05$; $p \geq 0.05$). In the EPVs, a significantly larger mean value was observed in the nasal quadrant compared to the inferior ($p \leq 0.05$), temporal ($p \leq 0.01$), and superior quadrants ($p \leq 0.01$) (Fig. 5B), but no significant differences in mean value were found between the temporal and superior quadrants ($p=0.081$) (Fig. 5B).

### 3.3 Differences in Outflow Structures in Active and Inactive Areas of Outflow

Confocal microscopy allowed us to analyze specific outflow structures and associate them with active or inactive outflow. First, we analyzed the TM and SC height. The TM was significantly thicker in areas of active outflow (103.3±4.0 μm; $p \leq 0.01$) compared to areas of inactive outflow (78.5±6.5 μm) (Fig. 6). This increase in TM thickness in active flow area did not significantly change SC height in active flow (13.3±0.67 μm) compared to inactive (11.4±1.02 μm) outflow areas ($p=0.135$).

We then analyzed number of collector channels. A summary of the total number of CCs and their associations with active and inactive outflow is presented in Table 2. A total of 80 CCs were counted in all frontal sections from 72 radial wedges. There was at least one CC found in 49 of 72 (68%) radial wedges, whereas no CCs were found in 23 of 72 (32%) radial wedges. A total of 63 CCs (79%) were found to be associated with areas of active outflow, whereas 17 CCs (21%) were found to be associated with areas of inactive outflow. Further analysis of CCs based on quadrants revealed that a larger number of CCs associated with active outflow were found in either the nasal (26 of 63, 41%) or inferior (20 of 63, 32%) quadrants with a smaller number found in the temporal (9 of 63, 14%) and superior (8 of 63, 13%) quadrants. CCs associated with inactive outflow were primarily found in the temporal (4 of 17, 23%) and superior (9 of 17, 53%) quadrants followed by the inferior quadrant (2 of 17, 12%) and nasal quadrant (2 of 17, 12%).

## 4. Discussion

This study used a combination of a newly developed global imaging method and confocal microscopy to investigate areas of active outflow in three distinct locations (TM, IW, and

EPVs) along the trabecular outflow pathway and to determine whether the segmental nature of aqueous outflow is conserved in the pathways distal to SC. Our main findings include: 1) a segmental nature of outflow is conserved distal to SC with variations found in the TM, IW, and EPVs; 2) mean EFA was similar along the IW and within EPVs; 3) preferential active outflow was observed in the nasal and inferior quadrants of the eye and was associated with a more expanded TM and higher number of CCs.

It is now believed that outflow within the TM and along the IW is segmental rather than uniform; however, in most previous studies, only a small portion of the trabecular outflow pathway was examined, and they were unable to provide outflow patterns on a whole eye perspective. Several recent studies have partially addressed these shortcomings by reporting a segmented pattern of outflow in the TM of whole eyes using montages of multiple confocal images, which was both time consuming and labor intensive (Keller et al. 2011, Chang et al. 2014, Vranka et al. 2015). However, these studies did not investigate outflow patterns distal to SC. Our current study was able to visualize outflow patterns in the TM and EPVs, for the first time, on a whole eye scale all within a single image using our global imaging technique. Additionally, when global imaging was used in tandem with confocal microscopy, we were able to demonstrate that the segmental pattern of outflow is conserved to EPVs from SC.

One question we would like to answer in this study is whether high tracer regions represent the high flow regions. It has been speculated that because tracers always flow to the areas with lower resistance, high tracer regions are high flow regions. However, it has also be argued that high tracer regions are low flow regions because the tracers became lodged. We found that in most of the areas where we observed the tracer particles in the EPVs, we also saw tracer particles reaching to the inner wall of SC from the inner TM. In most of the areas where no tracers were found in the TM, there were also no tracers found along the inner wall of SC and/or in EPVs. Our data led us to believe that areas of high tracer regions are high flow regions. It must be noted that in our classification of areas of active outflow, we included regions in which fluorescent tracer was observed in both the TM and along the IW. Tracer patterns in these areas could be attributed to either fluorescent tracers being prevented from moving past the IW or inadequate perfusion time for tracers to cross the IW endothelial layer.

Through comparison of areas of active outflow in three different locations (TM, IW, EPV), using our combined methods, a significantly higher EFA was found in the TM when compared to both the IW and EPVs, but no significant difference in EFA was found between the IW and EPVs. Compared to a previous study (Chang et al. 2014), our mean EFA value of the TM was higher (86±4% vs. 29±5%) (Mean±SD). This discrepancy may be explained by their perfusion of a smaller fixed volume (150μL) of two different tracers or the use of different imaging and measuring techniques. More specifically, Chang et al. (2014) calculated the tracer-labeled fraction of the TM based on pixel intensity, whereas our methodology measured active area by length. The same explanation could also apply to the difference observed when comparing IW EFA values of the two studies (21±6% vs. 35±3%). However, our IW EFA value is consistent with the control group of a previous human eye study (35±3% vs. 38±4%), which used a similar method (Yang et al. 2013). It is interesting

to note that a similar mean EFA was observed for both the IW and EPVs in this study, which suggests that although fluorescent tracer was observed in a larger area of the TM, a similar fraction of the tracer crossing the IW will continue on into EPVs.

Our investigation of which quadrant displayed more active outflow by analysis of fluorescent distribution and intensity in the TM and EPVs showed different results. In the TM, we did not find any one quadrant showing significantly more outflow. However, in EPVs, preferential flow was observed in the nasal and inferior quadrants (Fig. 5B). Similar to our observation, a previous study analyzing pigment particles in the TM also found a form of preferential flow, with particles located more often in the nasal and inferior quadrants (Hann and Fautsch 2009). We examined whether the needle tip was inserted towards only the nasal and inferior quadrants and found that was not the case. Therefore, we ruled out the possibility that preferential flow was an artifact due to the needle positioning in the eyes during perfusion. While we were able to observe distinct outflow patterns of the entire eye, one limitation of this study is that our perfusion study was performed in enucleated eyes in the supine position; unlike in vivo conditions, the effects of episcleral venous pressure, normal ciliary body tone, and position changes were not evaluated. Further *in vivo* studies will be needed to determine whether our findings reported here would be comparable to *in vivo* physiological condition. Another limitation for our classification of flow types for each wedge is the possibility that during perfusion fixation some fluorescent tracers may have been washed out. Collection of perfusate in future studies will allow us to determine precise amounts of tracers that were lost during fixation. Another limitation in this study is that fixed volume of fluorescent tracers was perfused into each eye, which limits our ability to see if outflow patterns in human eyes changes after perfusing for a longer period of time (>45 minutes). However, a previous perfusion study in human eyes (Johnson et al. 1990) showed that as perfusion time increased no significant difference in the percentage of latex microspheres passing through the outflow system was observed.

In order to understand what outflow structure(s) may contribute to segmental or preferential outflow, changes in the TM thickness, SC height, and prevalence of CCs and their relationship with active or inactive outflow were further investigated. While gross anatomical inspection of the TM shows very little differences along the circumference of the eye, previous reports indicate that the properties of the TM vary, along the circumference of the eye, by approximately 20% under light microscopy and as much as 31% under electron microscopy (Buller and Johnson 1994). Additionally, our previous studies in human eyes observed a thicker TM in regions of active outflow than in regions of inactive outflow (Yang et al. 2013). Similarly, our current study found that the TM is 25% thicker in areas of active outflow compared to areas of inactive outflow along the circumference of the eye. Expansion of the TM in the active flow areas did not appear to cause significant changes to SC height compared to inactive flow regions, which may indicate that the increased thickness occurred in the direction of the anterior chamber. This data suggests that preferential outflow is associated with regions with a more expanded TM, where a lower outflow resistance may exist.

Another outflow structure that we investigated are CCs, which was previously reported to be associated with preferential outflow in both bovine (Battista et al. 2008) and human eyes

(Hann and Fautsch 2009). Among all six eyes analyzed, we found a total of 80 CCs, which gave us an average of approximately 13 CCs per eye. This average number of CCs is lower than a previously reported number obtained from histological studies that used either serial sections (Dvorak-Theobald 1955, Rohen and Rentsch 1968) or 3D micro-CT (Hann et al. 2011). This could be due to the following three reasons: 1) Only approximately 70% (range 56–81%, SD=9%) of wedge of each eye was imaged by confocal microscopy, 2) CCs imaged using confocal microscopy do not have the same imaging capacity as light microscopy of serial histological sections or micro-CT, and 3) Some CCs may be located more anteriorly or posteriorly to the areas that we imaged by confocal microscopy. However, analysis of one eye processed to near completion (13 of 16 wedges) revealed a total of 16 CCs and an average of 1.23 CCs per radial wedge. Given the ability to process the final 3 wedges, we would see a total count of ~20 CCs, which is close to the total number of CCs found by Dvorak et al. (1955), who saw a range of 20 – 30 trunks (ostia) around the entire eye. Those CCs that were imaged and counted in this study presented an interesting distribution based on their type of outflow activity. The majority of CCs found were associated with areas of active outflow, and furthermore, the majority of CCs found in areas of active outflow were associated with the nasal or inferior quadrants. This partially coincides with a previous study that enumerated CCs and found a higher total number of CCs on the inferior portion of the eye (Dvorak-Theobald 1955). With a higher number of CCs in the nasal and inferior quadrants, this may suggest that these areas facilitate a higher-pressure drop from the TM to SC and provide a route of lower outflow resistance.

In summary, using a combination of the single global imaging method and confocal microscopy, our study confirms that the previously reported segmented pattern of outflow within the TM and along the IW is conserved in EPVs. A similarity in EFA between the IW and EPVs suggests that we can detect changes in the areas of active outflow in EPVs by using a simpler and less labor-intensive global imaging method in the future. Additionally, we found that active outflow is preferential to the nasal and inferior quadrants, which are also associated with both a more expanded TM and a higher number of CCs. The normal outflow patterns and variations along the outflow pathway reported in this study will provide the basis for future studies pertaining to changes in the eye with drug treatments, surgical device implants, and glaucoma.

## Acknowledgments

**Grant Support:** National Institute of Health Grant EY022634, The Massachusetts Lions Eye Research Fund

## References

Battista SA, et al. Reduction of the available area for aqueous humor outflow and increase in meshwork herniations into collector channels following acute IOP elevation in bovine eyes. Invest Ophthalmol Vis Sci. 2008; 49(12):5346–5352. [PubMed: 18515571]

Bill A. The aqueous humor drainage mechanism in the cynomolgus monkey (Macaca irus) with evidence for unconventional routes. Invest Ophthalmol. 1965; 4(5):911–919. [PubMed: 4157891]

Bill A, Hellsing K. Production and drainage of aqueous humor in the cynomolgus monkey (Macaca irus). Invest Ophthalmol. 1965; 4(5):920–926. [PubMed: 4157892]

Buller C, Johnson D. Segmental variability of the trabecular meshwork in normal and glaucomatous eyes. Invest Ophthalmol Vis Sci. 1994; 35(11):3841–3851. [PubMed: 7928181]

Chang JY, et al. Multi-scale analysis of segmental outflow patterns in human trabecular meshwork with changing intraocular pressure. J Ocul Pharmacol Ther. 2014; 30(2–3):213–223. [PubMed: 24456518]

de Kater AW, et al. Patterns of aqueous humor outflow in glaucomatous and nonglaucomatous human eyes. A tracer study using cationized ferritin. Arch Ophthalmol. 1989; 107(4):572–576. [PubMed: 2705927]

Dvorak-Theobald G. Further studies on the canal of Schlemm; its anastomoses and anatomic relations. Am J Ophthalmol. 1955; 39(4 Pt 2):65–89. [PubMed: 14361607]

Epstein DL, Rohen JW. Morphology of the trabecular meshwork and inner-wall endothelium after cationized ferritin perfusion in the monkey eye. Invest Ophthalmol Vis Sci. 1991; 32(1):160–171. [PubMed: 1987099]

Ethier CR, Chan DW. Cationic ferritin changes outflow facility in human eyes whereas anionic ferritin does not. Invest Ophthalmol Vis Sci. 2001; 42(8):1795–1802. [PubMed: 11431444]

Grant WM. Further studies on facility of flow through the trabecular meshwork. AMA Arch Ophthalmol. 1958; 60(4 Part 1):523–533. [PubMed: 13582305]

Grant WM. Experimental aqueous perfusion in enucleated human eyes. Arch Ophthalmol. 1963; 69:783–801. [PubMed: 13949877]

Hann CR, et al. Cationic ferritin and segmental flow through the trabecular meshwork. Invest Ophthalmol Vis Sci. 2005; 46(1):1–7. [PubMed: 15623746]

Hann CR, et al. Imaging the aqueous humor outflow pathway in human eyes by three-dimensional micro-computed tomography (3D micro-CT). Exp Eye Res. 2011; 92(2):104–111. [PubMed: 21187085]

Hann CR, Fautsch MP. Preferential fluid flow in the human trabecular meshwork near collector channels. Invest Ophthalmol Vis Sci. 2009; 50(4):1692–1697. [PubMed: 19060275]

Johnson M, et al. The filtration characteristics of the aqueous outflow system. Exp Eye Res. 1990; 50(4):407–418. [PubMed: 2338123]

Keller KE, et al. Segmental versican expression in the trabecular meshwork and involvement in outflow facility. Invest Ophthalmol Vis Sci. 2011; 52(8):5049–5057. [PubMed: 21596823]

Lu Z, et al. The Mechanism of Rho-Kinase Inhibitor, Y27632, on Outflow Facility in Monkey vs Human Eyes. Invest Ophthalmol Vis Sci. 2007; 48(5):1146.

Lu Z, et al. The mechanism of increasing outflow facility by rho-kinase inhibition with Y-27632 in bovine eyes. Exp Eye Res. 2008; 86(2):271–281. [PubMed: 18155193]

MacRae D, Sears ML. Peroxidase passage through the outflow channels of human and rhesus eyes. Exp Eye Res. 1970; 10(1):15–18. [PubMed: 4989613]

Maepea O, Bill A. The pressures in the episcleral veins, Schlemm's canal and the trabecular meshwork in monkeys: effects of changes in intraocular pressure. Exp Eye Res. 1989; 49(4):645–663. [PubMed: 2806429]

Maepea O, Bill A. Pressures in the juxtacanalicular tissue and Schlemm's canal in monkeys. Exp Eye Res. 1992; 54(6):879–883. [PubMed: 1521580]

Parc CE, et al. Giant vacuoles are found preferentially near collector channels. Invest Ophthalmol Vis Sci. 2000; 41(10):2984–2990. [PubMed: 10967055]

Rohen JW, Rentsch FJ. Morphology of Schlemm's canal and related vessels in the human eye. Albrecht Von Graefes Arch Klin Exp Ophthalmol. 1968; 176(4):309–329. [PubMed: 5305008]

Rosenquist R, et al. Outflow resistance of enucleated human eyes at two different perfusion pressures and different extents of trabeculotomy. Curr Eye Res. 1989; 8(12):1233–1240. [PubMed: 2627793]

Sabanay I, et al. H-7 effects on the structure and fluid conductance of monkey trabecular meshwork. Arch Ophthalmol. 2000; 118(7):955–962. [PubMed: 10900110]

Schuman JS, et al. Excimer laser effects on outflow facility and outflow pathway morphology. Invest Ophthalmol Vis Sci. 1999; 40(8):1676–1680. [PubMed: 10393035]

Scott PA, et al. Relationships between increased aqueous outflow facility during washout with the changes in hydrodynamic pattern and morphology in bovine aqueous outflow pathways. Exp Eye Res. 2009; 89(6):942–949. [PubMed: 19679123]

Swaminathan SS, et al. Secreted protein acidic and rich in cysteine (SPARC)-null mice exhibit more uniform outflow. Invest Ophthalmol Vis Sci. 2013; 54(3):2035–2047. [PubMed: 23422826]

Toris CB, et al. Aqueous humor dynamics in the aging human eye. Am J Ophthalmol. 1999; 127(4): 407–412. [PubMed: 10218693]

Vranka JA, et al. Mapping molecular differences and extracellular matrix gene expression in segmental outflow pathways of the human ocular trabecular meshwork. PLoS One. 2015; 10(3):e0122483. [PubMed: 25826404]

Yang CY, et al. Effects of y27632 on aqueous humor outflow facility with changes in hydrodynamic pattern and morphology in human eyes. Invest Ophthalmol Vis Sci. 2013; 54(8):5859–5870. [PubMed: 23920374]

Zhu JY, et al. Development of a novel two color tracer perfusion technique for the hydrodynamic study of aqueous outflow in bovine eyes. Chin Med J (Engl). 2010; 123(5):599–605. [PubMed: 20367989]

- Segmental nature of outflow is conserved in episcleral veins from Schlemm’a canal
- Areas of active outflow are associated with expanded trabecular meshwork
- Areas of active outflow are associated with more collector channels
- Preferential outflow occurs in the nasal and inferior quadrants

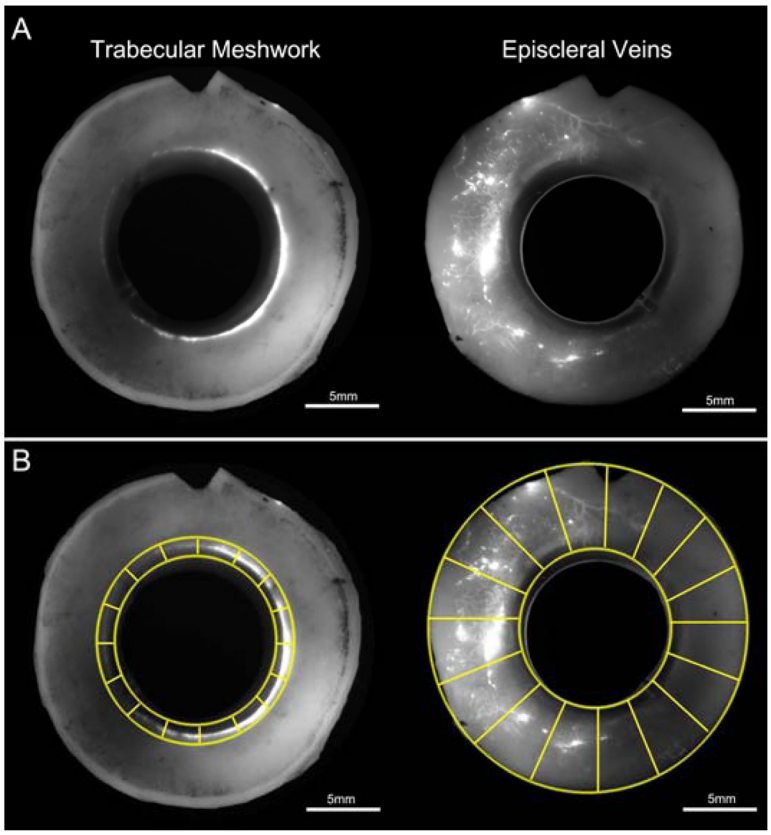


**Figure 1. Global Imaging of Normal Human Eyes**

A) Global image of anterior segments from a pair of normal human eyes that reveals fluorescent tracer patterns in the trabecular meshwork and episcleral veins. B) Digital separation of global images of the trabecular meshwork and episcleral veins into a minimum of 16 “wedges”.

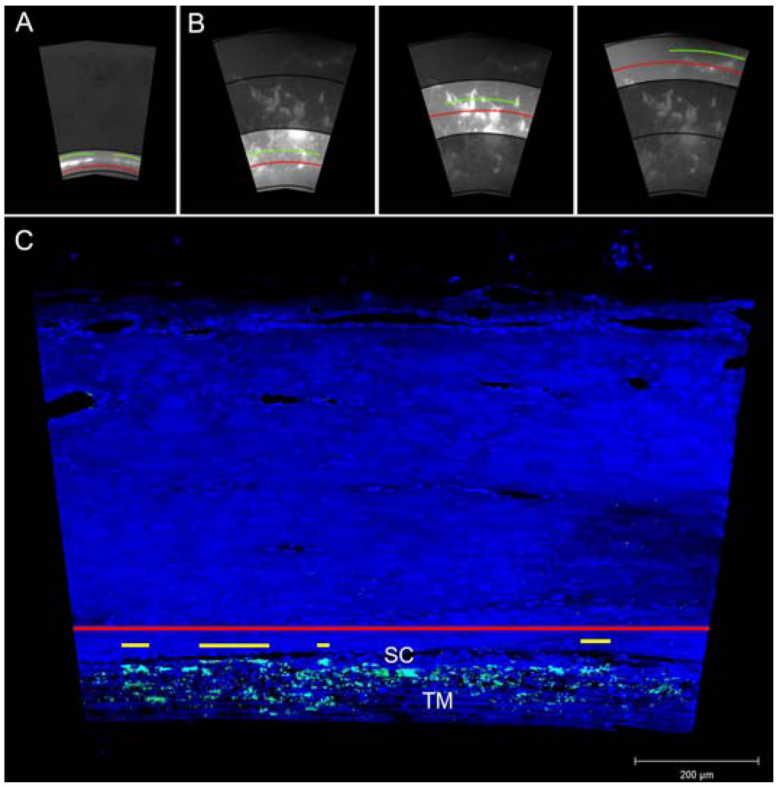


**Figure 2. Methods of Effective Filtration Area Measurements**

A) EFA measurement using global images of the TM. EFA was measured in only one region. The *red line* represents the total TM length and the *green line* represents the filtration length. TM EFA (ΣFL/ΣTSL) was calculated for each eye. B) EFA measurement using global images of EPVs. EFA was measured in three distinct regions. The *red line* represents the total scleral length and the *green line* represents the length of sclera labeled with fluorescent tracers. EPV EFA (ΣFL/ΣTSL) was calculated for each eye. C) Measurement of EFA (ΣFL/ΣTL) along the IW of Schlemm's canal using confocal images. The *red line* represents the total length of the IW and the *yellow line* represents fluorescent-decorated length of the IW. TM = trabecular meshwork; SC = Schlemm's canal.

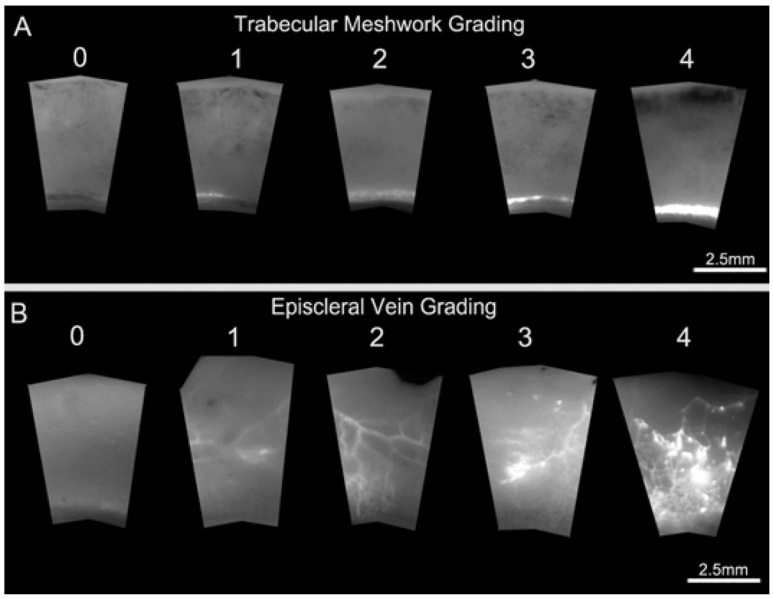


**Figure 3. Semi-Quantitative Evaluation of Fluorescent Tracer Distribution and Intensity**

A) Grading scale representative of variations of tracer distribution and intensity in the TM. "0" represents TM devoid of tracers and "1 – 4" represents a combination of increasing tracer distribution and intensity in the TM. B) Grading scale representative of variations of fluorescent tracer distribution and intensity in EPVs. "0" represents EPVs devoid of tracers and "1 – 4" represents a combination of increasing tracer distribution and intensity in EPVs.

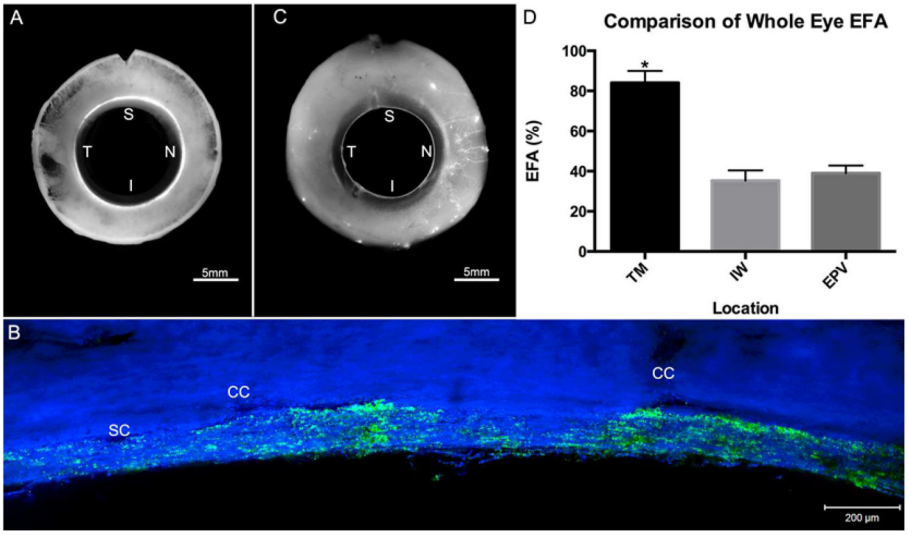


**Figure 4. Comparative Analysis of EFA in TM, IW, and EPVs**

A) A global image of the TM showing segmental tracer distribution. B) A confocal image of frontal sections from the same eye showing segmental tracer distribution along the IW with more tracer seen near collector channel (CC) ostia. C) Global image of EPVs showing a more segmented pattern of outflow than the TM. D) EFA of the TM showed a significantly (*) higher value (86.3±3.5%) compared to both the IW (34.7±2.9%; $p \leq 0.01$) and EPVs (41.1±3.8%) ($p \leq 0.01$). No significant difference was found between EFA values of the IW and EPVs ($p = 0.12$). SC = Schlemm's Canal; CC = Collector channel. S = Superior; N = Nasal; I = Inferior; T = Temporal

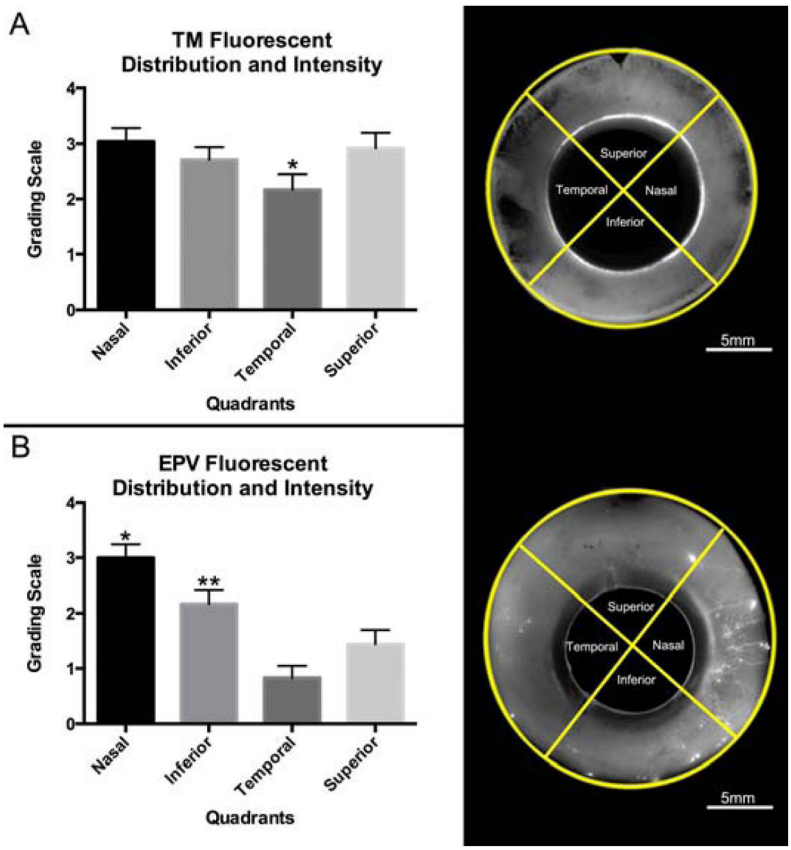


**Figure 5. Quadrant Analysis of Fluorescent Tracer Distribution and Intensity**

A) Active outflow in the TM, as shown by fluorescent tracer distribution, is more uniform across all quadrants. The temporal quadrant had a lower mean value than the superior, inferior, and nasal quadrant, but only reached statistical significance (*) with the nasal quadrant ($p \leq 0.05$). B) Active outflow as shown by fluorescent tracer distribution and intensity in EPVs is not equal between all quadrants. The nasal quadrant is significantly higher (*) in mean value compared to all other quadrants ($p \leq 0.05$). Inferior quadrant also shows a significantly higher (**) mean value compared to superior ($p \leq 0.05$) and temporal quadrants ($p \leq 0.01$). No significant difference in mean value was found between temporal and superior quadrant ($p = 0.081$).

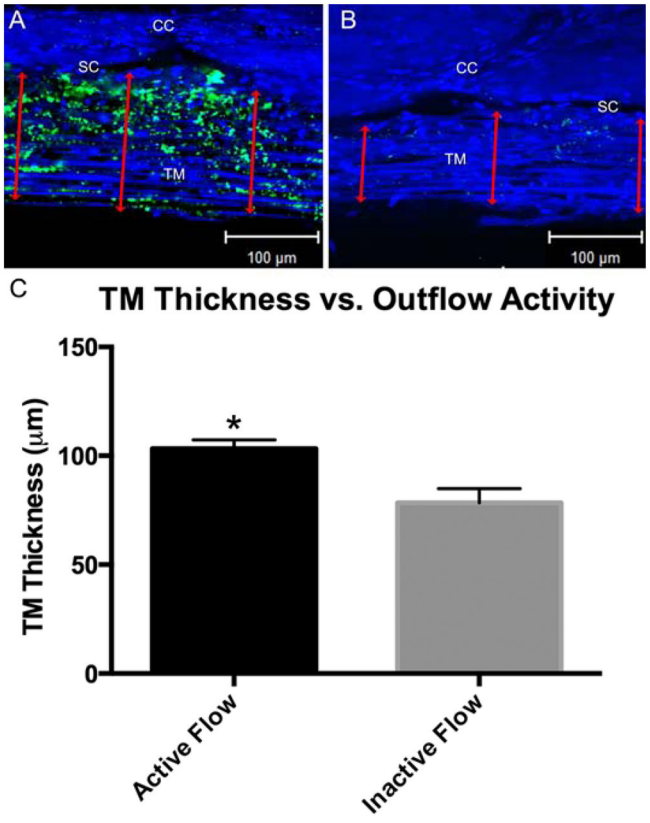


**Figure 6. Trabecular Meshwork Thickness in Areas of Active and Inactive Outflow**

A) In areas of active outflow more fluorescent green tracers within the TM and along the IW were observed as well as a thicker TM (red double arrows). B) Compared to active areas of outflow, inactive areas of outflow showed little to no green fluorescent tracers within the TM and along the IW as well as a thinner TM (red double arrows). C) TM thickness was significantly larger in areas of active outflow (103.3±4.0 µm; $p \leq 0.01$) compared to areas of inactive outflow (78.5±6.5 µm). CC = Collector channel; SC = Schlemm's canal; TM = Trabecular meshwork.

**Table 1**

Grading Scale for Fluorescent Distribution and Intensity

| **Trabecular Meshwork Grading Scale** |
|---|
| **0** No fluorescence |
| **1** < 50% dim fluorescence |
| **2** ≥ 50% dim fluorescence |
| **3** < 50% bright fluorescence |
| **4** ≥ 50% bright fluorescence |
| **Scleral Vein Grading Scale** |
| **0** No fluorescence |
| **1** < 50% dim fluorescence **OR** *< 20% bright fluorescent dots only* |
| **2** ≥ 50% dim fluorescence *with or without < 20% bright fluorescent dots* |
| **3** < 50% bright fluorescence |
| **4** ≥ 50% bright fluorescence |

**Table 2**

Collector Channel Analysis and Associations with Outflow Activity

| Outflow Activity | Tracers in TM | Tracers Along IW | Tracers in EPV | Total CCs | CCs in Nasal | CCs in Inferior | CCs in Superior | CCs in Temporal |
|---|---|---|---|---|---|---|---|---|
| **Active** | ✔ | ✔ | ✔ | 54 | 26 | 20 | 5 | 3 |
| **Active** | ✔ | ✔ | ✘ | 9 | - | - | 3 | 6 |
| **Inactive** | ✔ | ✘ | ✘ | 6 | - | 1 | 4 | 1 |
| **Inactive** | ✘ | ✘ | ✔ | 7 | 2 | - | 5 | - |
| **Inactive** | ✘ | ✘ | ✘ | 4 | - | 1 | - | 3 |

Outflow activity was based on the presence or absence of fluorescent tracers in three locations (TM, IW, and EPVs). Total of 80 collector channels were counted in the frontal sections from 72 different radial wedges. Majority of CCs associated with active outflow were found in the nasal (26 of 63) and inferior (20 of 63) quadrants. Majority of CCs associated with inactive outflow were found in the temporal (4 of 17) and superior (9 of 17) quadrants.